SOILS AND FOUNDATIONS Vol. 51, No. 5, 915–927, Oct. 2011
Japanese Geotechnical Society

EXPERIMENTAL INVESTIGATION OF LATERALLY LOADED PILES IN SAND UNDER MULTILAYERED CONDITIONS

JUNHWAN LEE[i], DOOHYUN KYUNG[ii], JUNGMOO HONG[iii] and DONGWOOK KIM[iv]

ABSTRACT

In the present study, the lateral load responses and the lateral load capacities of piles in sand under multilayered conditions were investigated. For this purpose, a series of lateral load tests using two model piles was conducted within a calibration chamber under various multilayered soil conditions. The test results were then compared with those obtained under uniform soil conditions. Using the test results, the effect of the multilayered soil conditions on the design components for laterally loaded piles, such as the pile rotation point, the ultimate lateral load capacity, and the lateral soil pressure profile, were analyzed. It was found that the lateral load responses of piles are largely affected by the soil conditions near the surface and the pile base, while the effect of the conditions in the middle-depth layers is relatively small. It was also observed that the depth to the pile rotation point fluctuates during the initial loading, but then becomes stabilized as the level of the load is increased. No significant difference in the depths to the pile rotation point was observed between the uniform and the multilayered soil conditions. Based on the test results in this study, a modified lateral pressure profile, applicable to the estimation of lateral pile load capacities, was proposed to more realistically reflect the effect of multilayered soil conditions.

Key words: earth pressure, failure, horizontal load, load test, model test, pile, sand (**IGC**: E4)

INTRODUCTION

The lateral load capacity of piles is an important design consideration for the construction of deep foundations. The lateral pile load capacity can be viewed from two different aspects, namely, the allowable lateral load capacity H_{all}, associated with the serviceability of superstructures, and the ultimate lateral load capacity H_u, associated with the failure of the surrounding soil or the pile itself. If a pile is sufficiently stiff and strong, compared to the surrounding soil, it is called a ''rigid'' or a ''short'' pile, and H_u is governed by the strength of the surrounding soil. For the estimation of H_u for rigid piles, it is necessary to identify the lateral soil resistance, p_u, and the distribution of the lateral soil pressure, p_L, along the embedded pile depth. Lateral soil resistance p_u is obtained at the fully mobilized passive stress state, while lateral soil pressure p_L is generally given as a certain portion of p_u. Once these two components have been identified, H_u can be calculated from the equilibrium condition of the resultant forces acting on the pile.

Various design methods have been proposed for the estimation of H_u (Broms, 1964; Petrasovits and Award, 1972; Reese et al., 1974; Prasad and Chari, 1999; Zhang et al., 2005; Schmertmann, 2006; Lee et al., 2010). However, the majority of these methods were developed for uniform soil conditions, assuming simplified linear or step-linear depth distributions of p_L. If the soil is nonhomogenous or is under multilayered conditions, the magnitude and the depth profile of p_L under such soil conditions will differ from those under uniform soil conditions. For example, in the methods by Petrasovits and Award (1972) and Prasad and Chari (1999), the pile rotation point, at which the stress reversal of active and passive conditions occurs, is introduced and its location needs to be identified for the calculation of H_u. Since the pile rotation point and the depth profile of p_L in these methods were proposed for uniform soil conditions, certain modifications would be necessary if multilayered soil conditions existed. In addition, as the effect of the sublayers on the magnitude and the profile variation in lateral resistance is not considered in the existing methods, the effect also need to be analyzed in detail and properly addressed in order to obtain more realistic predictions of the lateral pile load capacity.

In the present study, the lateral load responses and the load capacities of piles embedded in sand under multilayered conditions were investigated in comparison to those under uniform conditions. Lateral load tests using two model piles of different lengths, which were fully in-

[i] Professor, School of Civil and Environmental Engineering, Yonsei University, South Korea (junlee@yonsei.ac.kr).
[ii] Ph.D. Student, ditto (iamdh0630@yonsei.ac.kr).
[iii] Graduate Research Assistant, ditto (hong0710@yonsei.ac.kr).
[iv] Post-Doctoral Research Associate, Geotechnical Engineering Division, Korea Institute of Construction Technology (dwkim@kict.re.kr).
The manuscript for this paper was received for review on July 2, 2010; approved on May 20, 2011.
Written discussions on this paper should be submitted before May 1, 2012 to the Japanese Geotechnical Society, 4-38-2, Sengoku, Bunkyo-ku, Tokyo 112-0011, Japan. Upon request the closing date may be extended one month.

strumented, were conducted within a calibration chamber with sand specimens under both uniform and multilayered conditions. The sand specimens were prepared using the raining method to produce multilayered conditions with different relative densities. In order to characterize the test sand and the calibration chamber specimens, cone penetration tests were also conducted for each of the soil conditions considered in the lateral pile load tests. Based on the test results, the effect of the multilayered soil conditions on various design components, including the lateral soil pressure distribution, the lateral load capacity, and the pile rotation point, was analyzed. A modified lateral pressure distribution was proposed to more realistically reflect the effect of the multilayered soil conditions on the estimation of the lateral pile load capacity.

ESTIMATION OF LATERAL PILE LOAD CAPACITY

Property-based Approach

For the estimation of the ultimate lateral load capacity H_u of rigid piles, the following two key components should be identified, namely, lateral soil resistance p_u and a depth profile of lateral soil pressure p_L along the embedded pile depth. Lateral soil resistance p_u represents a unit lateral load capacity exerted by the surrounding soil, and it is typically obtained at the fully mobilized passive stress state. Lateral soil pressure p_L, on the other hand, is given as a certain portion of p_u and varies with depth. Different methods have been proposed for estimating p_u and p_L, mainly based on experimental test results (Broms, 1964; Petrasovits and Award, 1972; Barton, 1982; Prasad and Chari, 1999). In most of these methods, p_u is given as a function of internal soil friction angle ϕ' and vertical effective stress σ'_v, while p_L is assumed to show a simplified linear or a step-linear distribution along the embedded pile depth.

Figure 1 shows three representative methods for the estimation of H_u proposed by Broms (1964), Petrasovits and Award (1972), and Prasad and Chari (1999). In Broms's method, shown in Fig. 1(a), it is assumed that a pile rotates according to the pile base and that lateral soil pressure p_L is equal to p_u along the entire embedded pile depth. p_u in Broms's method is given as the following equation:

$$p_u = 3 \cdot K_p \cdot \sigma'_v \tag{1}$$

where K_p = Rankine's passive lateral stress ratio = $\tan^2(45 + \phi'/2)$, ϕ' = internal friction angle of the soil, and σ'_v = vertical effective stress. From the moment equilibrium condition, with respect to the pile base, H_u in Broms's method is obtained as

$$H_u = \frac{K_p \cdot \sigma'_{v,b} \cdot L^2 \cdot B}{2(e+L)} \tag{2}$$

where $\sigma'_{v,b}$ = vertical effective stress at the pile base level, L = embedded pile length, B = pile diameter, and e = vertical eccentricity of the lateral load from the soil surface. It should be noted that Eq. (2) is applicable only for uniform soil conditions that give a linear depth profile of p_u. When soils are under multilayered conditions, the depth profile of p_u is no longer linear, and the detailed p_u variation with depth needs to be identified.

Figures 1(b) and (c) show the methods by Petrasovits and Award (1972) and Prasad and Chari (1999), respectively. The equations for p_u in Petrasovits and Award's and Prasad and Chari's methods are given, respectively, as follows:

$$p_u = (3.7 \cdot K_p - K_a) \cdot \sigma'_v \tag{3}$$

$$p_u = 10^{(1.3 \tan \phi' + 0.3)} \cdot \sigma'_v \tag{4}$$

where K_a = Rankine's active earth pressure ratio = $\tan^2(45 - \phi'/2)$. As can be seen in Figs. 1(b) and (c), these methods include the pile rotation point, at which the direction of the passive stress state becomes reversed. In Prasad and Chari's method, the depth to the pile rotation point (d_r in Fig. 1) is given as a function of the embedded pile length (L) and the load eccentricity (e). d_r in Petrasovits and Award's method is obtained from trial-and-error iteration conducted until the equilibrium of the resultant forces acting on the pile surface has been reached. As these methods also assume uniform soil conditions, modifications to the distribution of p_L and the depth to the pile rotation point (d_r) are necessary when multilayered soil conditions are involved.

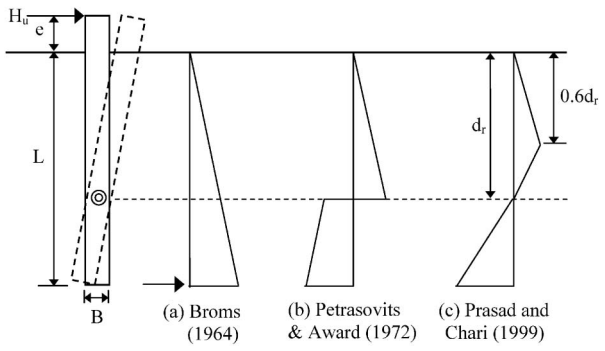

Fig. 1. Distributions of lateral soil pressure at ultimate state by (a) Broms (1964), (b) Petrasovits and Award (1972), and (c) Prasad and Chari (1999)

EXPERIMENTAL PROGRAM

Lateral Load Tests Using Model Piles

Lateral pile load tests were conducted with soil specimens prepared in a calibration chamber under both uniform and multilayered conditions. The diameter and the height of the calibration chamber were 77.5 and 125 cm, respectively. A schematic diagram of the chamber system (chamber with sand diffuser) is given in Fig. 2(a). In order to address the effect of pile length and different multilayer configurations on the lateral load response of a pile, two closed-ended steel-pipe model piles with different lengths equal to 90 and 56 cm were specifically manufactured and used in the tests. Both model piles were made of steel and had a diameter of 6 cm and a

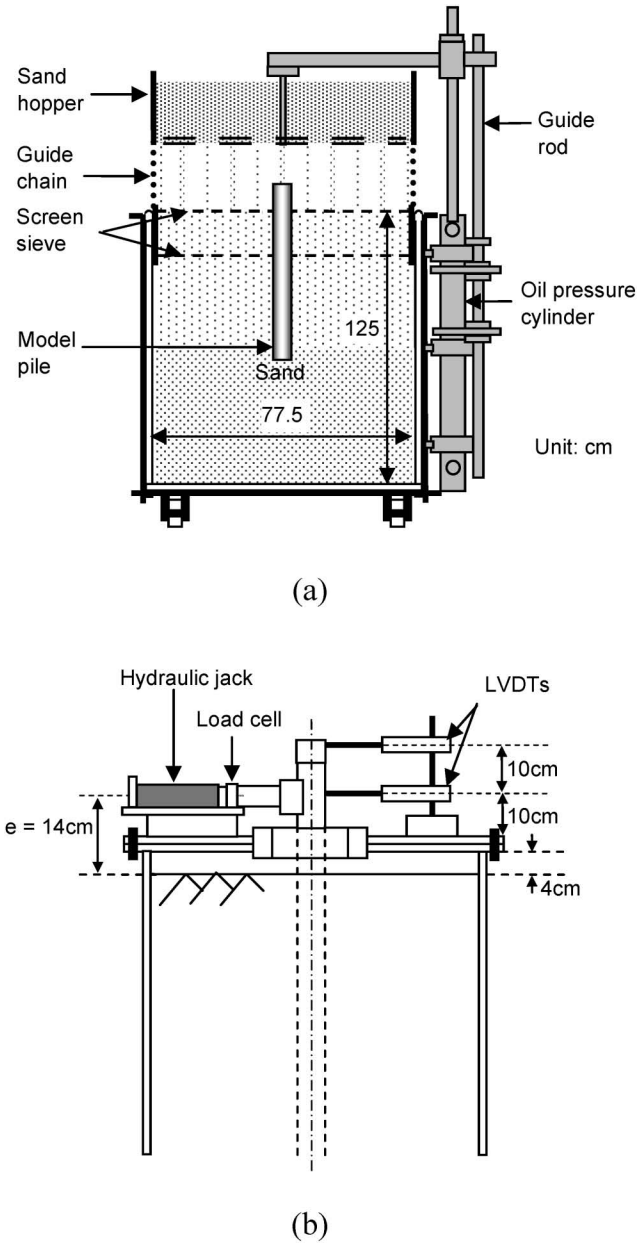

Fig. 2. Schematic diagram of calibration chamber test apparatus: (a) calibration chamber and (b) lateral loading device with LVDTs

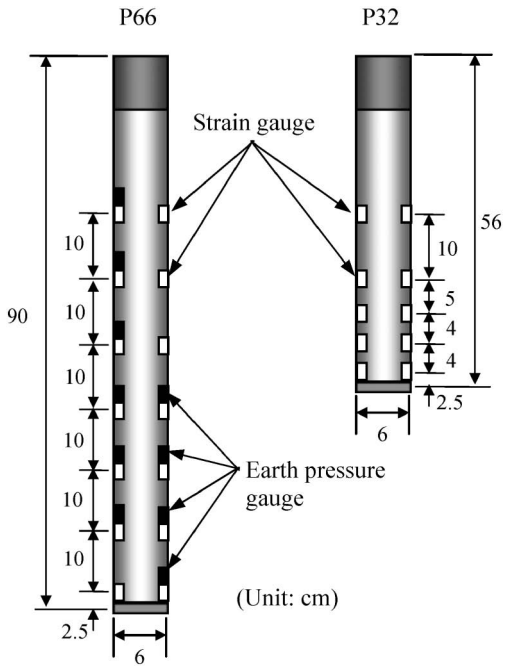

Fig. 3. Model piles used in calibration chamber lateral load tests

thickness of 0.37 cm. The elastic modulus of the model piles (E_p) was 350 GPa. When the piles were installed in the calibration chamber, the actual embedded depths of the piles were 66 and 32 cm, respectively. In the rest of this paper, these model piles will be referred to as P66 and P32, respectively. Details on the pile installation will be explained later.

As shown in Fig. 2(b), the soil surface of the specimen was located 4 cm below the top platen of the chamber. The upper 20 cm of the model pile, exposed above the top platen, was used for the installation of two LVDTs (Linear Variable Differential Transformers), set at different heights, and a lateral loading device. The lateral loading device and the lower LVDT were both installed 10 cm above the chamber's top platen, whereas the upper LVDT was set 20 cm above the top platen (i.e., 10 cm above the lower LVDT in the same measurement direction). Therefore, the vertical load eccentricity (e) was 14 cm.

Figure 3 shows the model piles (P66 and P32) used in the tests. Strain gauges were attached to the front and the rear sides of the piles, namely, 14 gauges for P66 and 10 gauges for P32. For P66, 6 earth pressure gauges were installed on the rear side and 4 gauges were installed on the front side of the pile to measure the lateral soil pressure acting on the pile upon loading. As can be seen in Fig. 3, some overlap of the earth pressure gauge alignments on both the front and the rear sides was allowed to ensure full coverage of the measurement of the passive soil pressure acting on the pile.

Calibration Chamber Specimens and Testing Procedure

The calibration chamber specimens were prepared using the raining method with a sand diffuser, composed of a sand container and two screen sieves. Two different relative densities of $D_R = 52$ and 92% were adopted for the preparation of the calibration chamber specimens. Therefore, the results obtained in this study are limited to the soil conditions of medium and dense states, and do not represent those of loose states. These two D_R values were selected as representative densities for foundation soils, since typical foundation soils are often in medium to dense states. The test sand was Jumunjin standard sand, a clean silica sand with the properties given in Table 1. The values for ϕ' were obtained from triaxial tests conducted under various soil conditions. Since different levels of confining stress were used in the triaxial tests, namely, in the range of 50–400 kPa, the ϕ' values in Table 1 are those that were averaged from the values obtained for different levels of confining stress. This indi-

Table 1. Properties of test sand

D_{10} (mm)	D_{60} (mm)	G_s	e_{max}	e_{min}	$\gamma_{d,max}$ (kN/m^3)	$\gamma_{d,min}$ (kN/m^3)	ϕ' ($D_R = 52\%$)	ϕ' ($D_R = 92\%$)
0.41	0.51	2.63	0.948	0.596	16.15	13.23	34.8°	37.8°

Table 2. Soil and test conditions

Pile Types	D_R of sub-layers	
	Uniform (D_R^1-D_R^2-D_R^3)	Multilayered (D_R^1-D_R^2-D_R^3)
P66 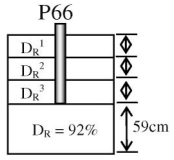	DDD, MMM	DDM, DMD MDD, MMD MDM, DMM
P32 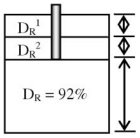	DD, MM	DM, MD

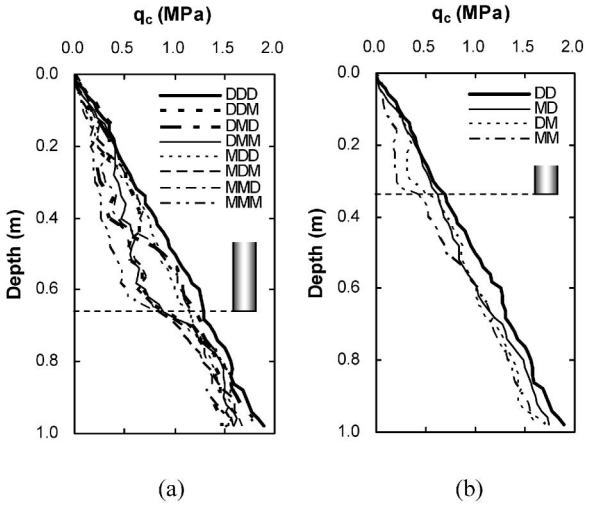

Fig. 4. CPT results for test specimens with different soil conditions for (a) P66 and (b) P32

cates that the friction angles given in Table 1 are likely to represent underestimated values compared to those in actual model tests that involved lower levels of confining stress. Multilayered soil specimens were prepared by forming several sub-layers with different relative densities. Table 2 summarizes the configurations and the combinations of soil layer conditions considered in the tests. In Table 2, the symbols 'M' and 'D' represent the medium and the dense states indicating $D_R = 52$ and 92%, respectively. A total of 12 cases, including 8 cases for P66 and 4 cases for P32, were adopted in the tests.

To prepare the calibration chamber specimens, sand was rained, namely, poured like rain, into the chamber maintaining a predetermined fall height, which corresponded to $D_R = 92\%$, until the bottom foundation soil layer was formed. The model pile was then placed and temporarily fixed with frames in the center of the bottom foundation soil. Once the model pile had been set, the raining of the sand was continued with an appropriate fall height corresponding to the target D_R for a given sublayer. When the model pile was sufficiently embedded in the sand, the frames were removed, and the sand raining was continued to finish the formation of the soil layers. When the installation of the model pile and the formation of the soil layers were complete, the stiff steel platen was placed over the top of the chamber upon which the lateral loading device and the LVDTs were installed, as shown in Fig. 2(b). The lateral loading device consisted of a hydraulic jack and a load cell with a 50-kN capacity. A load increment of 2 kN was initially applied, and then it was gradually reduced as the lateral deflection increased.

Cone Penetration Tests

Cone penetration tests (CPTs) were conducted for each of the 12 soil conditions adopted in the tests. The cone penetrometer used in this study consisted of a cone probe with extension rods, a pushing device, a depth encoder, and a data acquisition system. The cone probe was of a miniature type with a diameter and a cross-sectional area of 1.6 cm and 2.0 cm^2, respectively. The pushing device was specifically designed and manufactured; it consisted of a hydraulic jack with a 25-kN capacity, four steel bars, and a rod connection. Figures 4(a) and (b) show the results from the calibration chamber CPTs obtained under the different soil layer conditions for P66 and P32. As can be seen in Fig. 4(a), the q_c profiles for the uniform soil conditions (MMM and DDD) are approximately linearly bounding the lower and the upper limit ranges, while those for the multilayered conditions lie between them.

From Figs. 4(a) and (b), it is also observed that the differences in q_c values are less pronounced for the depths below the pile base than for those above the pile base. This is because the bottom foundation soil below the pile base was homogenous, formed with the same relative density of $D_R = 92\%$ for all cases, as indicated in Table 2. Therefore, the differences in q_c values in the foundation soil are only due to the differences in vertical stress with different unit weights from the multilayered soil layers above the pile base, while the differences in both D_R and stress within the multilayered soil layers are likely to produce a larger difference in q_c values.

TEST RESULTS AND ANALYSIS

Lateral Load Response

Figure 5 shows the lateral load-displacement curves obtained for P66 (Figs. 5(a) and (b)) and P32 (Fig. 5(c)).

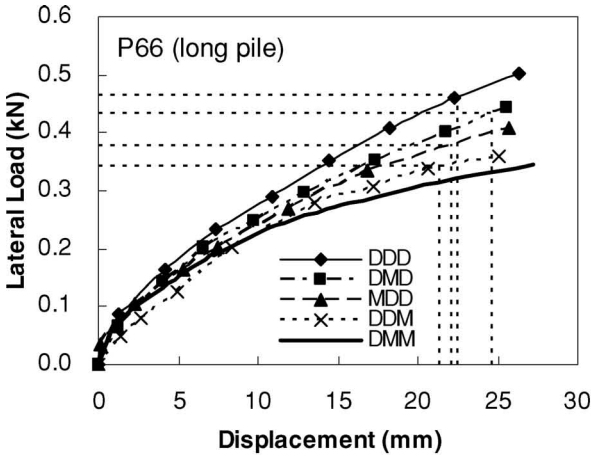

(a)

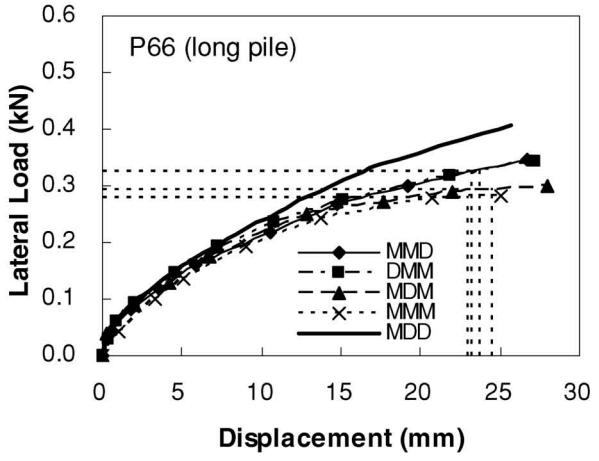

(b)

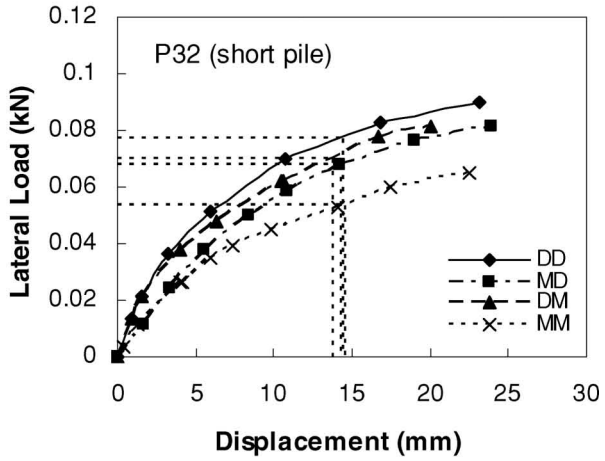

(c)

Fig. 5. Lateral load-displacement curves for (a) P66 with more than two dense layers, (b) P66 with more than two medium layers, and (c) P32

The intersections between the horizontal dashed lines and the y-axes in the figures indicate ultimate lateral load capacity H_u, which will be described in further detail later. For P66, due to the many combinations of soil conditions, the test results were categorized into two groups, as plotted in Figs. 5(a) and (b), for a clearer description of the test results. Figure 5(a) shows the results for the specimens with more than 2 dense ($D_R = 92\%$) layers, while Fig. 5(b) includes those with more than 2 medium ($D_R = 52\%$) layers. The results for DMM and MDD were also included in Figs. 5(a) and (b), respectively, as reference plots. From Fig. 5(b), it is seen that the load-displacement curves for MMM and MDM are fairly close, indicating that the effect of the middle-depth layers is not significant. This can also be observed from other cases with two comparable soil conditions, as shown in Fig. 6. It is seen that the effect of the soil conditions of the middle layers on the lateral load response of a pile is overall insignificant for all the cases. As can be found from Fig. 5, however, the effect of the upper and the lower layers was quite significant. This will be discussed in the next section.

Figure 7 shows the depth distributions of the bending moments (M) for P66. While P32 was also instrumented, the strain measurements obtained from P32 were found to be erroneous, and therefore, were not included herein. As expected, the highest and the lowest bending moments were observed for DDD and MMM, respectively. It is also observed that the maximum bending moments occurred at a depth of around 0.24 m below the soil surface, corresponding to 0.36 times the embedded pile depth. Similar results were obtained for all other cases of uniform and multilayered soil specimens. This implies that if soils were in medium to dense states, no significant difference in depths to the maximum bending moment would be observed between uniform and multilayered soil conditions.

Ultimate Lateral Load Capacity

Load-settlement criteria, used to define the axial pile load capacities, have been well established (Davisson, 1972; Franke, 1989; Lee and Salgado, 1999). For laterally loaded piles, limited information is available, while some criteria, mainly related to specific structure types and design considerations, have been adopted in practice (Meyerhof et al., 1981; Fleming et al., 1992; El Naggar and Wei, 1999; Zhihong et al., 2006; Lee et al., 2010). Among them, lateral load-deflection criteria, acceptable for general design purposes, can be found from Meyerhof et al. (1981), GAI Consultant Inc. (1982), and Haldar et al. (1997). According to Meyerhof et al. (1981), ultimate lateral load capacity H_u can be defined as the load at which the lateral deflection starts to increase approximately linearly with the increasing lateral load. GAI Consultant Inc. (1982) and Haldar et al. (1997) specified H_u as the load corresponding to a pile rotation angle equal to 2°. According to Lee et al. (2010), the values for H_u defined by Meyerhof et al. (1981) closely match those obtained from the 2° criterion. In this study, the 2°

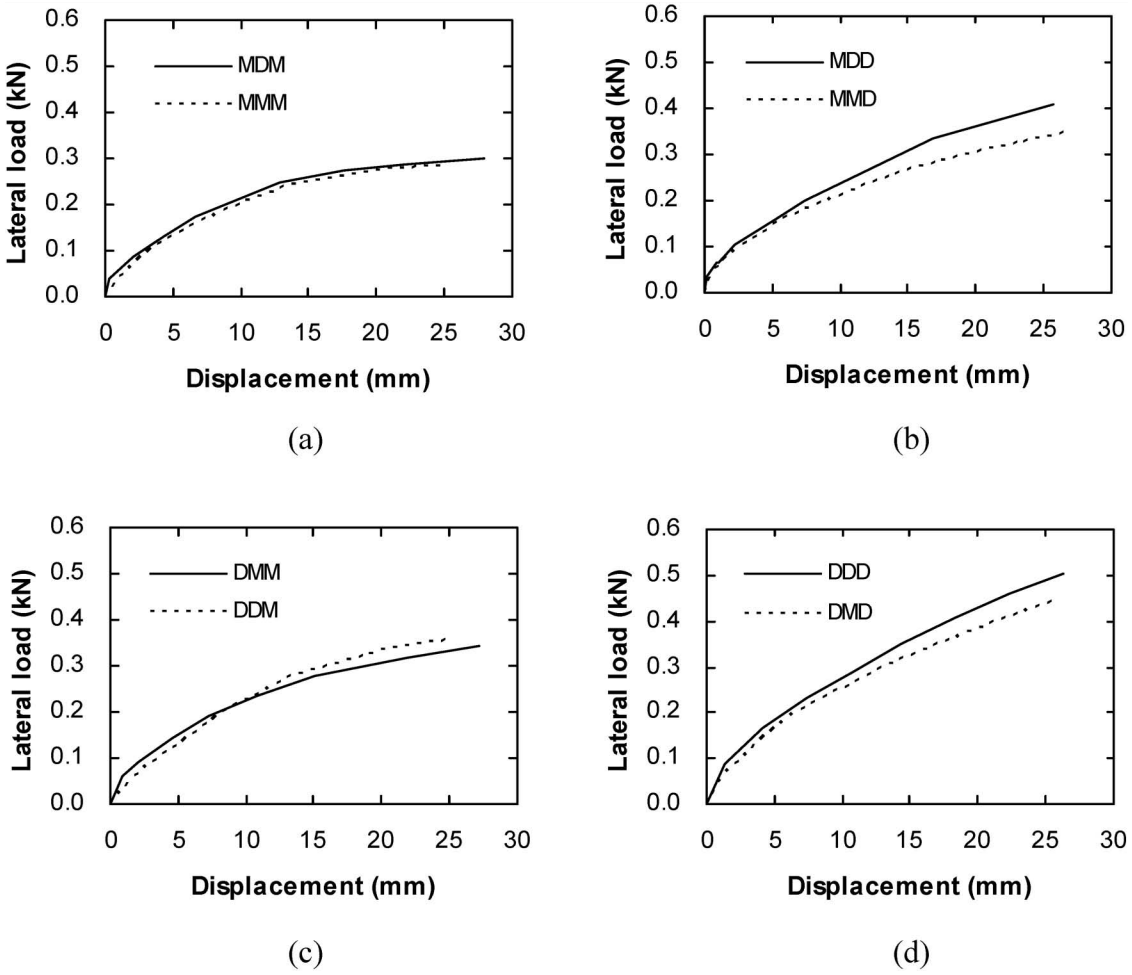

Fig. 6. Effect of middle layers on lateral load response for soil conditions of (a) MDM-MMM, (b) MDD-MMD, (c) DMM-DDM, and (d) DDD-DMD

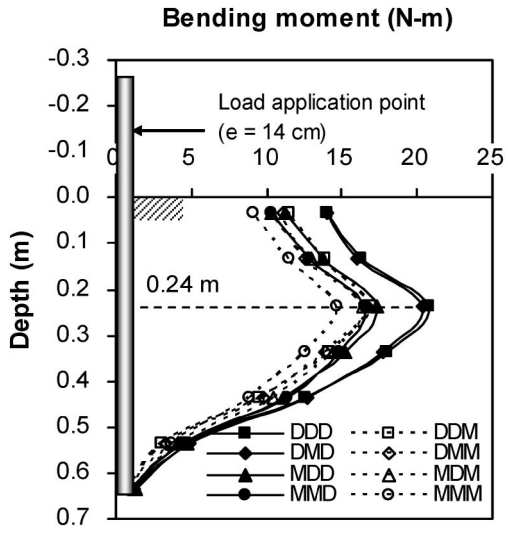

Fig. 7. Distributions of bending moments for test piles

criterion has been adopted to determine H_u, since it is more straightforward and easier to specify H_u on load-deflection curves. As two lateral displacements were measured from the lower and the upper LVDTs at a vertical distance of 10 cm (Fig. 2(b)), it was possible to measure uniquely the 2° rotation angle of the model piles upon lateral loading. The values for H_u, obtained using the 2° criterion, are shown in Fig. 5, as indicated by the horizontal dashed lines.

Figure 8 shows the H_u values for different multilayered conditions. In Fig. 8(a), the values for H_u are compared for different D_R values of the top layer (given as "x"), whereas Figs. 8(b) and (c) represent similar comparisons for the middle and the bottom layers, respectively. As shown in Fig. 8(b), no significant difference in H_u is observed for the change in D_R of the middle layer. The effect of the top and the bottom layers on H_u, as observed from Figs. 8(a) and (c), however, is quite noticeable. They show larger H_u values for higher D_R values of the layers.

Pile Rotation Point

As described in Fig. 1, piles show rotational behavior upon lateral loading. While Broms's method does not consider the rotational behavior of piles, the methods by Petrasovits and Award (1972) and Prasad and Chari (1999) take into account the pile rotation point for the calculation of H_u. For Petrasovits and Award's method, the depth to the pile rotation point (d_r) is searched itera-

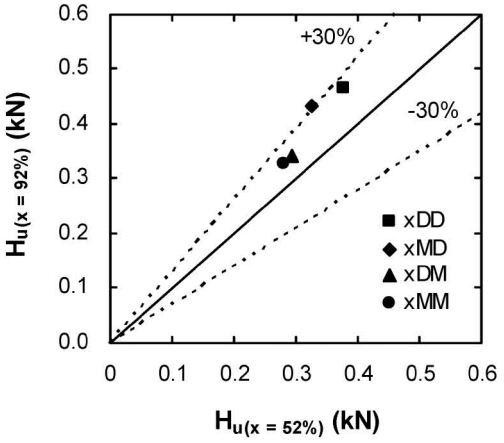

(a)

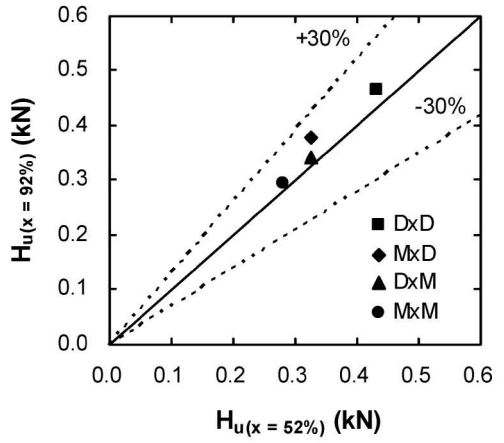

(b)

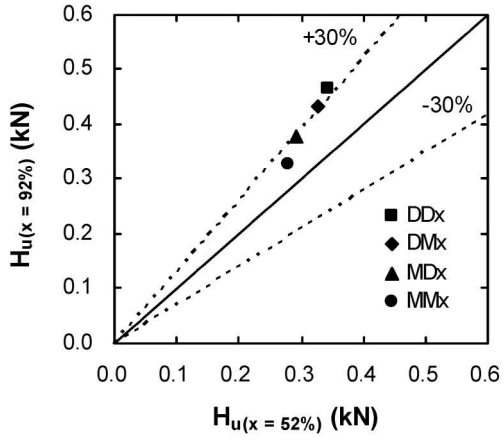

(c)

Fig. 8. Comparison of H_u values according to D_R variations in (a) top layer, (b) middle layer, and (c) bottom layer

tively until a force equilibrium condition is satisfied. In Prasad and Chari's method, on the other hand, d_r is calculated using the following equation:

Table 3. Values of rigidity ratio for different soil conditions

Pile	E_p (MPa)	I_p (mm^4)	Soil Layer Condition	E_s (MPa)	L (mm)	K_r
P32	350000	73532	DD	0.82	320	2.991
			MD	0.74	320	3.312
			DM	0.60	320	4.091
			MM	0.31	320	7.910
P66	350000	73532	DDD	1.67	660	0.081
			MDD	1.35	660	0.100
			DMD	1.24	660	0.109
			MMD	1.19	660	0.114
			DDM	1.22	660	0.111
			MDM	1.15	660	0.118
			DMM	1.10	660	0.123
			MMM	0.67	660	0.202

$$\frac{d_r}{L} = \frac{\sqrt{7.29(e/L)^2 + 10.541(e/L) + 5.307} - (2.7(e/L) + 0.567)}{2.1996} \quad (5)$$

where L = embedded pile length and e = load eccentricity. It is noted that, although the calculated (Eq. (5)) and the measured d_r values have been found to match well, no specific consideration for multilayered conditions is included.

Since two LVDTs were installed on the model piles used in this study, it was also possible to identify the depth to the pile rotation point, assuming that the piles were sufficiently stiff compared to the surrounding soil. Once the pile rotation angle is obtained from the two LVDT measurements, the depth to the pile rotation point can also be identified geometrically by comparing the original and the inclined positions of the pile. In order to confirm the relative rigidity of the pile, the following rigidity ratio proposed by Meyerhof (1995) was adopted:

$$K_r = \frac{E_p I_p}{E_s L^4} \quad (6)$$

where K_r = relative rigidity ratio, E_p = elastic modulus of the pile, I_p = 2nd order cross-sectional moment of the pile, E_s = elastic modulus of the soil, and L = embedded pile depth. According to Meyerhof (1995), a pile can be regarded as rigid if K_r is greater than 0.01. The values of K_r for the model piles are given in Table 3. In Table 3, the values of E_s for the soil were estimated using the E_s-q_c correlation by Schmertmann et al. (1978) ($E_s = 2.5\ q_c$) with cone resistance values averaged for the embedded pile depths from the CPT results shown in Fig. 4. It can be seen that the values of K_r for all the model pile cases are high enough for them to be considered rigid.

Figure 9 shows the variations in normalized depth to

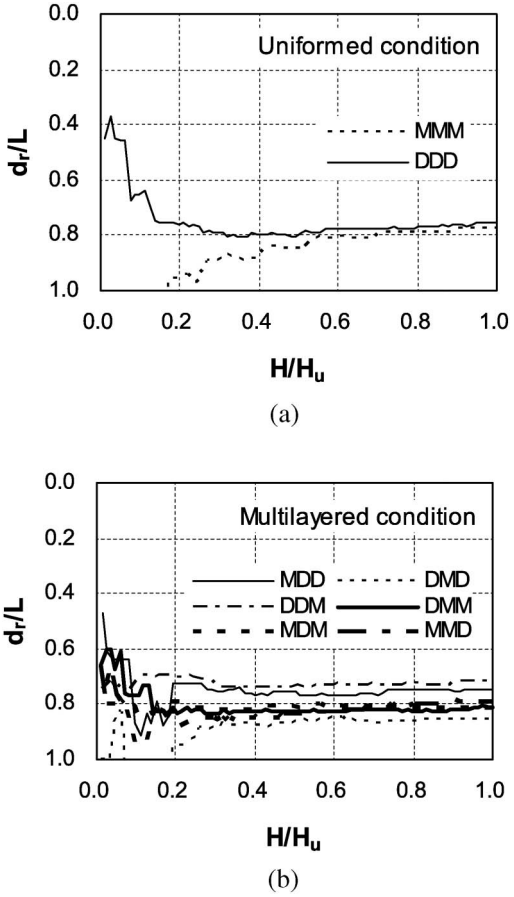

Fig. 9. Variations in normalized depth to pile rotation point (d_r/L) according to normalized lateral load (H/H_u) for (a) uniform soil conditions and (b) multilayered soil conditions

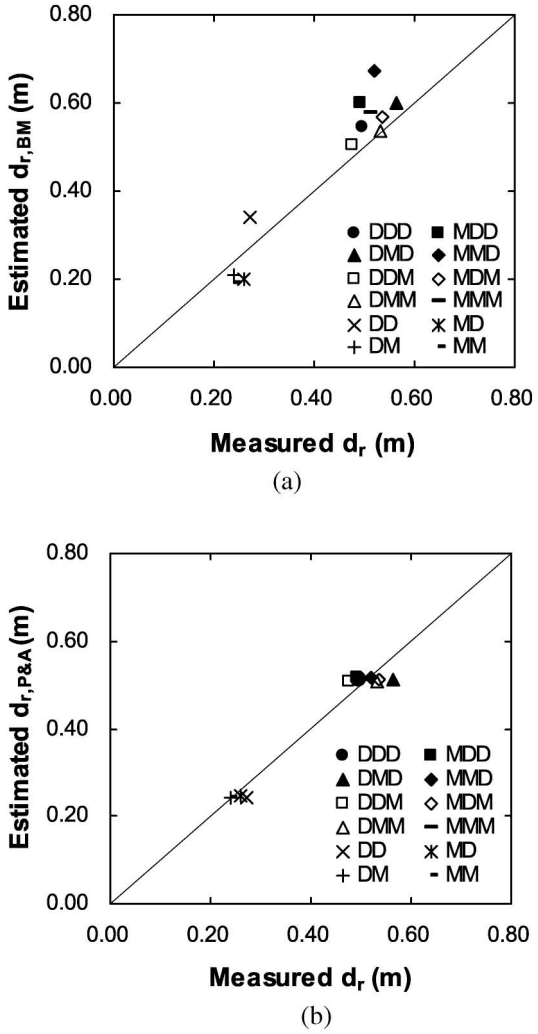

Fig. 10. Measured versus estimated values for d_r with (a) bending moment method and (b) Petrasovits and Award's method

the pile rotation point (d_r/L) according to the normalized lateral load (H/H_u) for uniform (Fig. 9(a)) and multilayered (Fig. 9(b)) conditions. It is seen that d_r/L under both conditions fluctuates initially, and then becomes stabilized. For the uniform conditions in Fig. 9(a), d_r tends to converge after $H/H_u \approx 0.2$ at $d_r/L \approx 0.76$. For the multilayered conditions in Fig. 9(b), different values for d_r/L at $H = H_u$ are observed in the range of 0.72–0.85. However, the variation in d_r appears to be fairly limited, indicating that the effect of the multilayered conditions on d_r is small and that a similar calculation procedure for d_r may be applicable for both uniform and multilayered conditions. Note that this observation is valid only for soil in medium to dense states, as considered in this study.

In order to further analyze the pile rotation point, three different methods were adopted to estimate d_r. These are Petrasovits and Award's method, Prasad and Chari's equation of Eq. (5), and the bending moment method based on the results in Fig. 7. For the bending moment method, lateral soil pressure $p(z)$ was obtained by the second-order differentiation of bending moment M with respect to depth z, namely,

$$p(z) = \frac{d^2M(z)}{dz^2} \tag{7}$$

where $p(z)$ = lateral soil pressure at a certain depth z and $M(z)$ = bending moment at a certain depth z. Once $p(z)$ is obtained from Eq. (7), d_r can be obtained as a depth where $p(z) = 0$.

Figure 10 shows measured versus estimated d_r values at $H = H_u$. In Fig. 10, $d_{r,\,BM}$ and $d_{r,\,P\text{ and }A}$ represent those from the bending moment method and Petrasovits and Award's method, respectively. From Fig. 10(a), it is seen that the values for d_r from Eq. (7) match those measured reasonably well, while some overestimated d_r values are observed for P66 under MDD and MMD conditions (notice that both of these cases include dense bottom layers). Figure 10(b) shows measured versus calculated d_r values using Petrasovits and Award's method. Values for d_r from Prasad and Chari's method using Eq. (5) were calculated as 50 and 23.5 cm for P66 and P32, respectively. Since no soil properties are involved in Eq. (5), values for d_r from Prasad and Chari's method are given as constants. For both uniform and multilayered conditions, the calculated d_r values show a close match to the measured values. It is also seen that these values agree well with the results from Prasad and Chari's method.

Based on these results, it can be summarized that no dramatic changes in the pile rotation point seem to occur for multilayered soil conditions, while some were observed for the density conditions of the medium to dense states. This, in turn, indicates that the existing methodology for the d_r estimation, proposed for uniform soil conditions, may also be used for multilayered soil conditions in practical applications.

COMPARISON WITH EXISTING DESIGN METHODS

Measured and Calculated Lateral Load Responses

Accurately estimating the depth distribution of lateral soil pressure p_L, acting on a pile, is a key design factor in estimating ultimate lateral load capacity H_u. In this study, they were measured directly from the tests and compared with those calculated using existing design methods. Figure 11 shows the p_L distributions at $H = H_u$, measured and calculated, for uniform (Fig. 11(a)) and multilayered (Fig. 11(b)) soil conditions. It is seen that the measured p_L distributions match those calculated using Prasad and Chari's method reasonably well for both uniform and multilayered soil conditions.

The depths to the maximum lateral soil resistance were observed at depths of around 0.4–0.5 d_r, which are smaller than 0.6 d_r proposed by Prasad and Chari's method. As discussed by Guo (2008), the depth of the maximum lateral soil pressure may vary depending on the displacement level. Theoretically, it approaches d_r if sufficiently large lateral displacements are allowed and if the passive state is fully mobilized along the entire embedded pile depth. Such conditions would then be identical to those specified in Petrasovits and Award's method, as shown in Fig. 1(b). The other noticeable aspect is that no significant difference in the p_L distributions is observed between the uniform and the multilayered soil conditions. As shown in Fig. 11(b), the p_L distributions for different multilayered conditions are quite similar, while MMD shows a somewhat exceptional distribution shape.

Figure 12 shows the measured versus the calculated ultimate lateral load capacities (H_u). For both uniform and multilayered soil conditions, the calculated H_u values were higher than the measured values. In particular, the tendency to overestimate was more pronounced for cases with lower D_R conditions in the bottom layers. In both

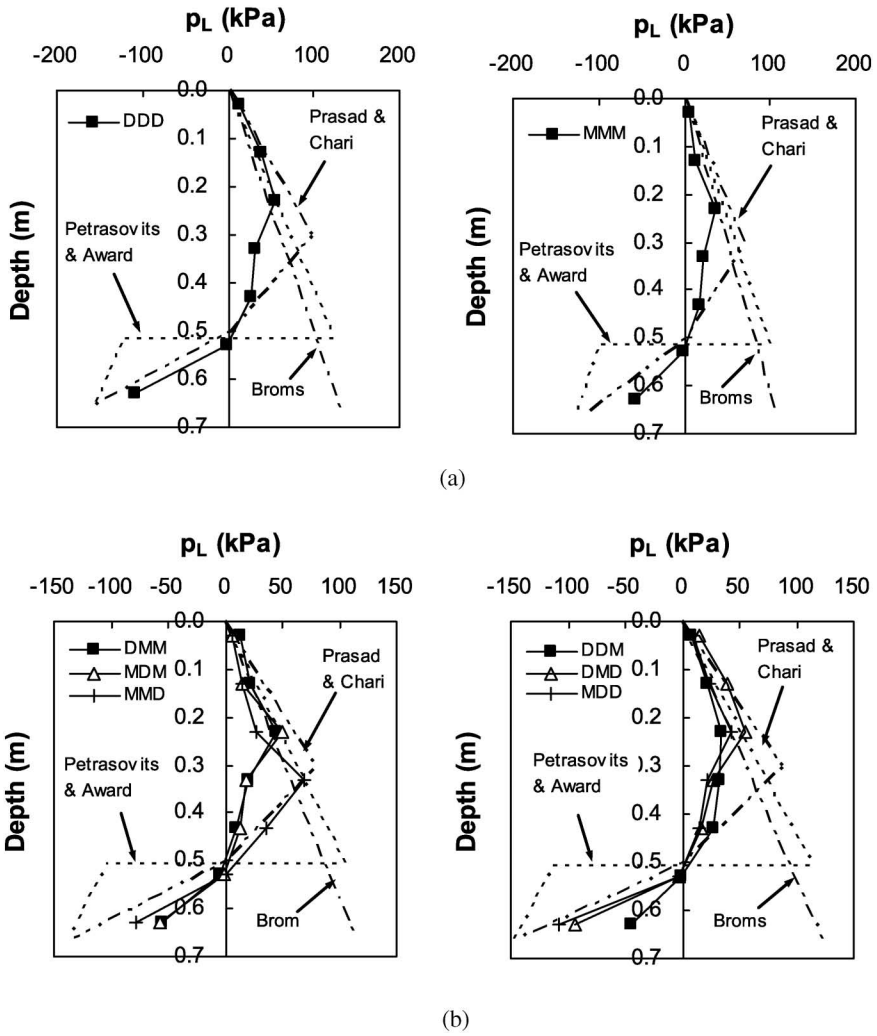

Fig. 11. Depth profiles of p_L for (a) uniform conditions and (b) multilayered conditions

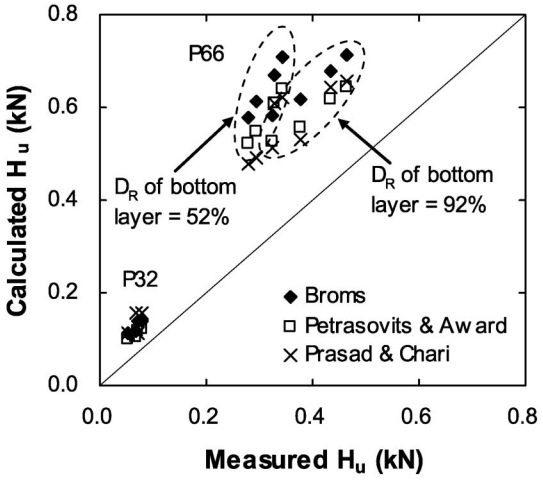

Fig. 12. Comparison between measured and calculated ultimate lateral load capacities

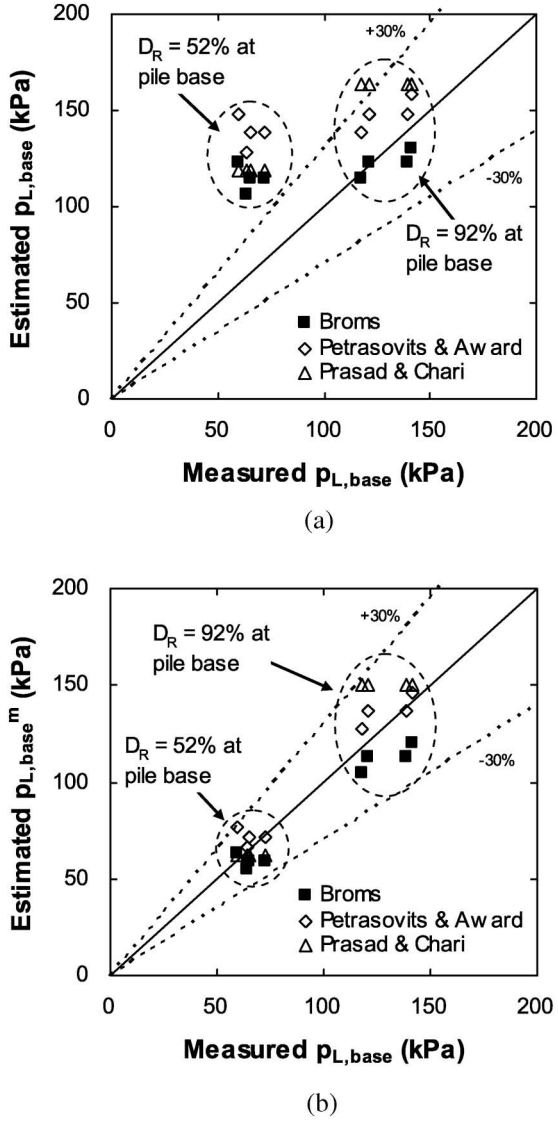

Fig. 13. Comparison of lateral soil pressure at pile base with (a) original methods and (b) D_R correction

Broms's and Petrasovits and Award's methods, the lateral soil resistance at the pile base ($p_{L,\,base}$) is assumed to be equal to p_u. In Prasad and Chari's method, $p_{L,\,base}$ is given as 1.7 times the p_u obtained at the depth of 0.6 d_r. Experimental evidence has shown that this assumption is reasonably acceptable for uniform soil conditions (Prasad and Chari, 1999). For multilayered conditions, however, this assumption may result in errors, since the actual soil conditions at the pile base, independent of the soil conditions at 0.6 d_r, are not taken into account for the calculation of $p_{L,\,base}$.

Figure 13(a) shows the measured and the calculated values for $p_{L,\,base}$. As indicated in Fig. 13(a), all the methods considered in this study overestimate $p_{L,\,base}$ when $D_R = 52\%$ at the pile base, while a reasonable match, at least in an approximate manner, is observed when $D_R = 92\%$. Note that H_u in this study is defined with a pile rotation angle of 2°. The results in Fig. 13(a) indicate that the fully mobilized passive state of the soil near the pile base has not been reached yet for $D_R = 52\%$, and that more lateral movements of the pile would be required for the full mobilization of p_u. This can be confirmed from the depth profiles of p_L for DDD and MMM shown in Fig. 11(a).

The test results obtained in this study suggest that modifications would be necessary if the effect of the soil conditions on $p_{L,\,base}$ are to be properly considered for the estimation of H_u. Based on the test results and the D_R effect shown in Fig. 13(a), therefore, the following modified relationship is introduced:

$$p^{m}_{L,\,base} = p_{L,\,base} \cdot I_D \tag{8}$$

where $p^{m}_{L,\,base}$ and $p_{L,\,base}$ = the modified and the original lateral soil resistance at the pile base, respectively, and I_D = relative density index = $D_R/100$. Note that Eq. (8) is an empirical equation, obtained from the test results given in Fig. 13(a), and thus, it is valid for the soil conditions considered in this study. Values for $p_{L,\,base}$ were recalculated using Eq. (8) and compared with the measured values in Fig. 13(b). From the figure, it is seen that the values for $p^{m}_{L,\,base}$ using Eq. (8) show an improved match to the measured values.

Effect of Sub-layer Soil Conditions

The significant effect of the top and the bottom layers on the lateral load response of piles is an important finding obtained in this study. To compare this finding with the results from existing design methods, a set of multilayered soil conditions was assumed and used to calculate H_u. Three sub-layers, namely, top, middle, and bottom, were assumed, and the effect of each layer on H_u was investigated employing different D_R values. A total of 48 conditions were assumed and used to calculate H_u for this comparison. The values for the soil unit weight and the friction angle adopted in this investigation and in the calculation of H_u are given in Table 4.

Figure 14 shows the variations in H_u with respect to D_R of the upper, the middle, and the bottom layers, as indi-

Table 4. Soil friction angles and unit weights

D_R (%)	ϕ'	γ (kN/m^3)
30	33.2°	14.00
50	34.6°	14.55
70	36.1°	15.15
90	37.6°	15.80

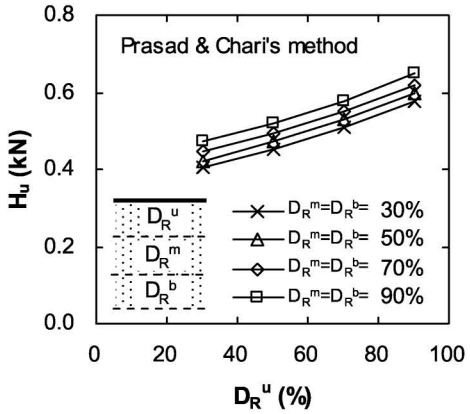

(a)

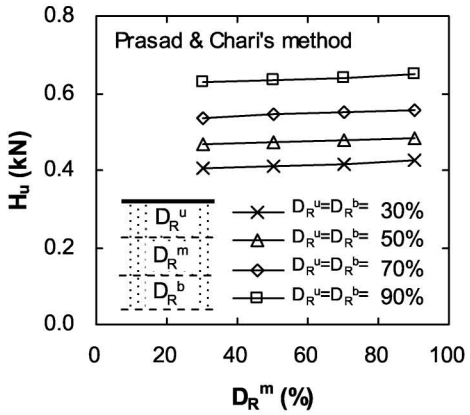

(b)

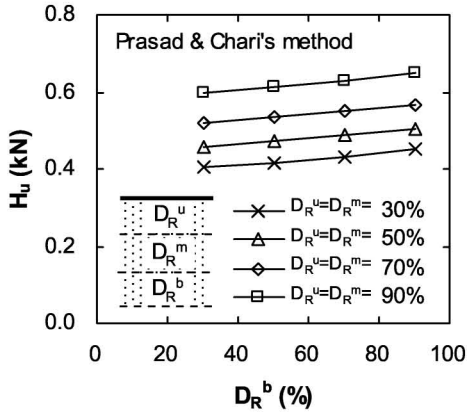

(c)

Fig. 14. Variations in H_u according to D_R changes in (a) top, (b) middle, and (c) bottom layers

cated by D_R^u, D_R^m, and D_R^b, respectively. The values for H_u in Fig. 14 were obtained using Prasad and Chari's method. It is seen that the effect of the upper layer (Fig. 14(a)) is quite noticeable, showing an increasing H_u with an increasing D_R. The effects of the middle and the bottom layers (Figs. 14(b) and (c)), however, were relatively small. A similar tendency was also obtained using Petrasovits and Award's and Broms's methods, although these results are omitted in the present paper. This trend is certainly different from the trend which was observed from the calibration chamber tests where the effect of the bottom layers was found to be significant. Therefore, when conventional design methods are adopted for multilayered soil deposits, it is strongly suggested that the multilayer effect on the lateral load response of the piles, in particular for the bottom layers, be properly addressed.

Modified Lateral Soil Pressure Distribution

Prasad and Chari's method is known to better represent the actual distribution of lateral soil pressure p_L, since the partial mobilization of the lateral soil resistance is taken into account (Schmertmann, 2006) in this method. However, when multilayered soil conditions are involved, the method still represents some uncertain aspects, as discussed previously, because the calculation of H_u is independent of the conditions of the bottom layers. In this section, to more realistically reflect the multilayer effect, a modification of Prasad and Chari's original method is proposed. The focus of this modification is put on the lateral soil pressure distribution in the bottom layer zones below the pile rotation point.

Figure 15 shows the depth profiles of p_L (solid lines) and p_u (dashed lines) for Prasad and Chari's method. In this figure, three p_u profiles below the depth of d_r are

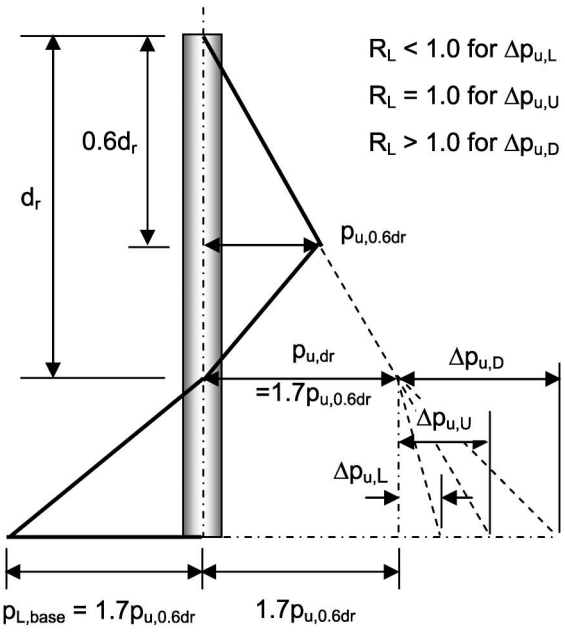

Fig. 15. Depth profiles of p_L and p_u for uniform and multilayered conditions

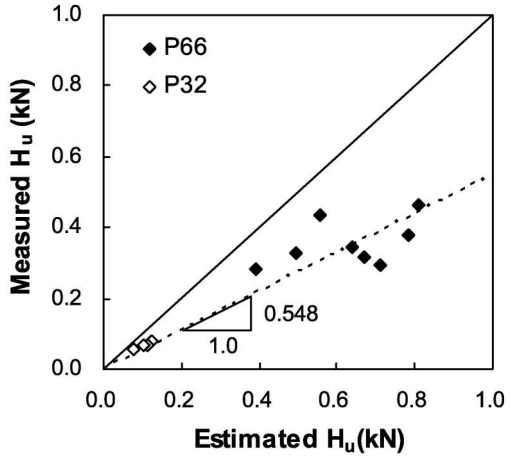

(a)

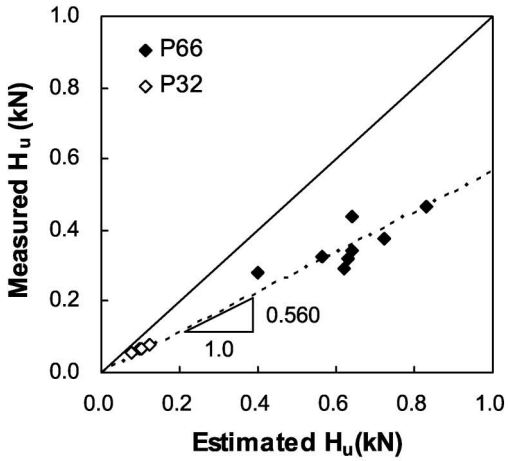

(b)

Fig. 16. Measured versus calculated H_u values with (a) original and (b) modified p_L profiles

given, corresponding to looser, uniform, and denser conditions. As illustrated in Fig. 15, p_u at the pile base can be broken down into $1.7\,p_{u,\,0.6dr}$ and Δp_u. For the looser, uniform, and denser conditions of the soil layers below the pile rotation point, Δp_u is given as $\Delta p_{u,\,L}$, $\Delta p_{u,\,U}$, and $\Delta p_{u,\,D}$, respectively. In order to represent the variation and the effect of the bottom layer conditions, the ratio of Δp_u to that for the uniform soil conditions can be defined as follows:

$$R_L = \frac{\Delta p_u}{\Delta p_{u,\,U}} \tag{9}$$

where R_L = lateral resistance ratio, Δp_u = lateral soil resistance component for a given bottom layer condition, and $\Delta p_{u,\,U}$ = lateral soil resistance component for the uniform soil conditions. For uniform soils, R_L is equal to 1; it represents the same p_L profile as that given in Prasad and Chari's original method. According to Prasad and Chari's original method for uniform soils with $R_L = 1$, $p_{L,\,base}$ is equal to $1.7\,p_{u,\,0.6dr}$ (or $p_{u,\,dr}$). Therefore, for multilayered conditions, $p_{L,\,base}$ can be modified and estimated using R_L as follows:

$$p_{L,\,base} = R_L \cdot (p_{u,\,dr}) \tag{10}$$

If Eq. (10) is combined with Eq. (8), $p^{m}_{L,\,base}$ is given as follows:

$$p^{m}_{L,\,base} = I_D \cdot R_L \cdot (p_{u,\,dr}) \tag{11}$$

Figure 16 shows the values of the measured and the calculated H_u using the original (Fig. 16(a)) and the modified (Fig. 16(b)) p_L profiles. The dashed lines in Figs. 16(a) and (b) represent the best fit lines with gradients of 0.548 and 0.560, respectively. It is found that both the original and the modified approaches overestimate H_u in comparison to the measured values. However, it is seen that the results from the modified p_L profile show an improved match with less data scatter.

SUMMARY AND CONCLUSION

In the present study, the lateral load responses and the lateral load capacities of rigid piles in sand were investigated with focus on those under multilayered soil conditions. For this purpose, lateral load tests using model piles were conducted within a calibration chamber under uniform and multilayered soil conditions. In order to systematically analyze the effect of the multilayered conditions, two model piles, which were fully instrumented and had different lengths and different sub-layer conditions, were used in the calibration chamber tests. For each of the calibration chamber specimens, CPTs were conducted as well.

From the test results, it was found that when a pile is embedded in a multilayered soil deposit, the lateral load response of the pile is largely affected by the soil conditions of the top and the bottom soil layers, while the effect of the conditions of the middle-depth layers is relatively small. It was also observed that the maximum bending moment occurs at a depth of around 0.36 times the embedded pile length for both uniform and multilayered conditions.

The depth to the pile rotation point (d_r) was measured, and its variation was analyzed according to the multilayered soil conditions. The test results showed that despite the initial fluctuation of d_r, it eventually converged to the range of 0.72–0.85 times the pile length. Values for d_r, obtained from Prasad and Chari's method, were in good agreement with the measured values for both the uniform and the multilayered soil conditions.

The measured p_L distributions showed close matches to those proposed by Prasad and Chari (1999). From the comparison between the measured and the calculated H_u values using Prasad and Chari's method, it is seen that the method overall overestimated the H_u values for both the uniform and the multilayered conditions. The degree of overestimation was different, however, depending on the D_R of the bottom layer. Based on the test results, a modified p_L distribution for Prasad and Chari's method was proposed reflecting the actual soil conditions below the pile rotation point. The proposed modification consists of two parts. One is the modified p_L equation at the

pile base that can reflect the relative density at the pile base. The other is the modified p_L distribution profile, below the pile rotation point, that can consider the effect of the multilayered conditions.

From a comparison of the results obtained using Prasad and Chari's original method and those obtained using the proposed modification, it was found that both approaches overestimated H_u in comparison to the measured values, while the proposed modification showed less data scatter. This implies that further research may be necessary to investigate the discrepancy between the measured and the calculated H_u values and to improve the accuracy of the predictions. The application of a CPT-based method, such as the one proposed by Lee et al. (2010), for a better evaluation of the lateral load capacity of rigid piles under multilayered conditions, is also an option for future research.

ACKNOWLEDGEMENT

This work was supported by Basic Science Research Program through the National Research Foundation of Korea (NRF) grant funded by the Korea government (MEST) (No. 2011–0030845).

REFERENCES

1) Barton, Y. O. (1982): Laterally loaded model piles in sand: Centrifuge tests and finite element analyses, *Ph.D. Thesis*, University of Cambridge.
2) Broms, B. B. (1964): Lateral resistance of piles in cohesionless soils, *J. Soil Mech. and Found. Div.*, **90**(3), 123–158.
3) Davisson, M. T. (1972): High capacity piles, *Proceedings of Lecture Series on Innovations in Foundation Construction*, ASCE, Illinois Section, Chicago, March **22**, 81–112.
4) El Naggar, M. H. and Wei, J. Q. (1999): Responses of tapered piles subjected to lateral loading, *Canadian Geotechnical J.*, **36**, 52–71.
5) Fleming, W. G. K., Weltman, A. J., Randolph, M. F. and Elson, W. K. (1992): *Piling Engineering*, John Wiley and Sons, Inc., New York.
6) Franke, E. (1989): Large diameter piles, *Co-report to discussion, Session B, 12th ICSMFE*, Rio de Janeiro, Brazil.
7) GAI Consultant Inc. (1982): *Laterally Loaded Drilled Pier Research* Vol. 2, Research Documentation GAI Report EL–2197, Research Project 1280–1, California.
8) Guo, W. D. (2008): Laterally loaded rigid piles in cohesionless soil, *Canadian Geotechnical J.*, **45**(5), 676–697.
9) Haldar, A., Chari, T. R. and Prasad, Y. V. S. N. (1997): Experimental and analytical investigation of directly embedded steel pile foundation, Canadian Electricity Association, Montreal, Que., *Research Report* CEA 384T971.
10) Lee, J. and Salgado, R. (1999): Determination of pile base resistance in sands, *J. Geotech. Geoenv. Eng.*, **125**(8), 673–683.
11) Lee, J., Kim, M. and Kyung, D. (2010): Estimation of lateral load capacity of rigid short piles in sands using CPT results, *J. Geotech. Geoenv. Eng.*, **136**(1), 48–56.
12) Meyerhof, G. G., Mathur, S. K. and Valsangkar, A. J. (1981): Lateral response and deflection of rigid wall and piles in layered soils, *Canadian Geotechnical J.*, **18**, 159–170.
13) Meyerhof, G. G. (1995): Behavior of pile foundations under special loading conditions: 1994 R. M. Hardy keynote address, *Canadian Geotechnical J.*, **32**(2), 204–222.
14) Petrasovits, G. and Award, A. (1972): Ultimate lateral resistance of a rigid pile in cohesionless soil, *Proceedings 5th European Conference on SMFE 3*, Madrid, 407- 412.
15) Prasad, Y. V. S. N. and Chari, T. R. (1999): Lateral capacity of model rigid piles in cohesionless soils, *Soils and Foundations*, **39**(2), 21–29.
16) Reese, L. C., Cox, W. R. and Koop, F. D. (1974): Analysis of laterally loaded piles in sand, *Proceedings 6th Offshore Technology Conference*, **2**, 407–412.
17) Schmertmann, J. H., Hartman, J. P. and Brown, P. R. (1978): Improved strain influence factor diagrams, *Journal of the Geotechnical Engineering Division*, ASCE, **104**(GT8), 1131–1135.
18) Schmertmann, J. H. (2006): Discussion of ultimate lateral resistance to piles in cohesionless soils, *J. Geotech. Geoenv. Eng.*, **132**(8), 1108–1109.
19) Zhang, L., Silva, R. and Grismala, R. (2005): Ultimate lateral resistance to piles in cohesionless soils, *J. Geotech. Geoenv. Eng.*, **131**(1), 78–83.
20) Zhihong, H., McVay, M., Bloomquist, D., Herrera, R. and Lai, P. (2006): Influence of torque on lateral capacity of drilled shafts in sands, *J. Geotech. Geoenv. Eng.*, **132**(4), 456–464.